# I
# Materials

## A
## Donors

*Organic Photovoltaics: Materials, Device Physics, and Manufacturing Technologies.*
Edited by Christoph Brabec, Vladimir Dyakonov, and Ullrich Scherf

ISBN: 978-3-527-31675-5

# 1

# Regioregular Polythiophene Solar Cells: Material Properties and Performance

*Paul C. Ewbank, Darin Laird, and Richard D. McCullough*

## 1.1

## Introduction

Structural optimization of polymeric semiconductor devices is a fundamental problem for organic electronic materials. Transport properties necessitate controlling molecular orientation to maximize electronic connectivity and properties in a device. For example, electrodes in solar cells are orthogonal to those in field effect transistors, requiring efficient transport in different dimensions of a thin film, and may optimize differently. In addition, semiconductive polymers are blended with acceptors molecules that add yet another parameter in the structural optimization in organic photovoltaics or solar cells. In this context, organic photovoltaics (OPV) are studied to understand materials properties, optimize device parameters, and minimize cost. We focus on head-to-tail (HT) regioregular poly(3-alkylthiophene)s (rr-PAT or HT-PAT). Earlier reviews have focused on polymer synthesis and structure [2–4] or conjugated polymer based devices [5–9]. Herein, we seek to merge current understanding of HT-PAT structure and morphology with the material specific properties exploited in OPV devices. It is important to understand the details of rr-PT structure, so that optimization of donor/acceptor blends can be optimized. Tracing the path from single molecules through aggregation in solution to deposition of solid phases, we try to understand the morphological effects of purification, characterization, deposition, annealing, and other process modifications. Performance of HT-PT in OPVs is surveyed in the context of this assembly model.

### 1.1.1

### Overview of Nomenclature and Synthesis

Facile synthesis, ease of modification, and performance make polythiophenes the most versatile and extensively studied conjugated polymer in electronic devices. Irregular placement of side chain functional groups bestows solubility and tractability but at a cost: steric interactions arise, limiting backbone conformation and modes

*Organic Photovoltaics: Materials, Device Physics, and Manufacturing Technologies.*
Edited by Christoph Brabec, Vladimir Dyakonov, and Ullrich Scherf

ISBN: 978-3-527-31675-5

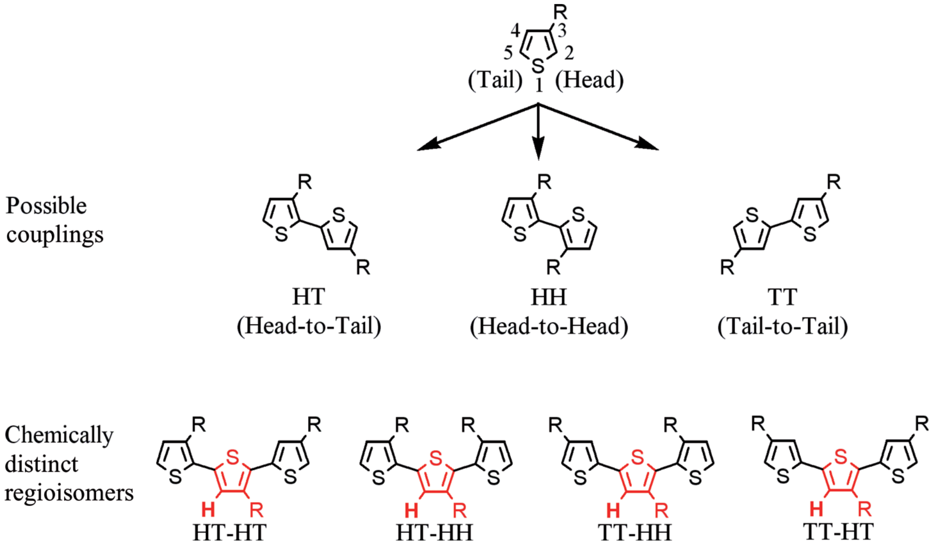

**Figure 1.1** Coupling regiochemistry.

of molecular association. At the extreme, twisting of the backbone of the conjugated polymer limits effective conjugation length, widening the HOMO (highest occupied molecular orbital)–LUMO (lowest unoccupied molecular orbital) gap while forming nonplanar conformers that cannot associate with efficient intermolecular orbital overlap. Studies on 3-functional thiophenes found that controlling regiochemistry during synthesis minimizes deconjugation. Nomenclature of polythiophenes has been developed to distinguish coupling isomers. By convention, the sterically crowded 2-position of the asymmetric monomer is designated the “head” (H) and the less hindered 5-position the “tail” (T) (Figure 1.1). Joining two rings can yield three isomeric dimers, HT, HH, or TT, with different steric environments. Regiochemistry is commonly quantified as the proportion of couplings or coupling sequences enchained. For example, a 51-mer with 49 HT couplings and 1 TT defect would be 98% HT. Note that the proportion of a single defect changes with the degree of polymerization and may be undetectable in large chains. Other common prefixes seen in the literature include “rr” or “rR” for any regioregular polythiophene with HT content >90%, and “ir” (irregular), “rIR” (regioirregular), or “ran” (random) for <90%. A statistically randomly coupled PT has been reported for only one protocol [10]. To avoid confusion, we limit our use of “ran” to this product. The smallest chemically distinct sequences within a chain, a thiophene ring and its two neighbors, are denoted by the coupling regiochemistry in the triad (Figure 1.1). The desired HT–HT regioisomer dominates in all PAT except ran-PT.

For alkyl derivatives the HH isomer is severely congested, requiring significant energy (>5 kcal) to force planarity [2–4]. In the HH isomer case, properties dependent on efficient π-stacking, including conduction and charge mobility, are disrupted. Random incorporation leads to variable sequence length distributions [11], limiting the size of polymer segments capable of π-stacking and their oxidation potential. In contrast, HT and TT isomers can easily access planarity or can adopt slight twists in the solid state, since up to 20° twist at the HT or TT junction is found in a shallow potential well (>1 kcal) in energy surface calculations. Defect-free HT architectures can stack at all points along the polymer chain. Domains develop from long, low oxidation potential segments with reorganization energy, the "cost" of structural changes stabilizing oxidation or reduction of the π-system, rendered negligible [12].

The synthesis of PTs falls into two distinct classes: oxidative coupling (chemically or electrochemically) and metal-assisted cross-coupling reactions. Oxidative couplings lead to HT enriched sequences, with $FeCl_3$ polymerization typically yielding ~70% HT–HT, not a statistically random distribution of the four triads. Control is possible exploiting electronic effects that localize charge, directing reactivity of the monomer, but is severely limited to select functionality. Metal-assisted cross-couplings are more versatile with selectivity derived from the metal-monomer adduct. Functional group tolerance may be altered by choice of coupling protocol. Coupling selectivity depends on the size of the metal and bulk of its ligands [10]. It can be tuned from a statistically random to a quasi "living" process, giving HT-regiospecificity for all but one coupling ($HT_n$–TT) along with narrow polydispersity and targeted molecular weight [13–15]. Several highly selective and efficient metal-assisted cross-coupling polymerizations produce HT-regioregular 2,5-coupled architectures from asymmetric monomers and are reviewed elsewhere in detail [2–4,16].

### 1.1.2
### Advantages of the HT Architecture

The benefits of the predominantly HT architecture are immediately apparent in PATs. Easily accessible planar conformations add new dimension to structural organization, with aggregation and stacking extending electronic connections across molecular ensembles. Self-assembly is inherent, preventing disorganized agglomeration under common processing conditions. Plasticization of alkyl chains by suitable solvent allows reorganization and segregation of the aromatic backbone from aliphatic substituents, forming π-stacks of linearly extended molecules – even in solution. The drive to self-assemble is a specific function of the HT architecture. However, in films cast quickly from solvent, trapping chains in a nonequilibrium state can be found, leading to large internal tensile strain [17]. Irregular PT neither develops strain nor spontaneously forms ordered structures. Slow casting deposits strain-free films. Processing conditions can bias π-stack orientation parallel to a surface, with linear [18] or radial [19] symmetry, or perpendicular to a surface [20]. Nanorods or fibers can be formed with domains oriented parallel [21] or perpendicular [22] to the long axis. Crystalline needles several hundred micrometers long have been reported [23,24]. Such well-defined organization of organic semiconductors is exploitable for building electronic devices on a molecular level and should be taken into account in device optimization.

## 1.2
## Assembly and Morphology

Aggregation and assembly of solid-state structures can be rationalized from a simple associative model (Figure 1.2). Molecular conformation, determined by solvation, prefigures association [30]. Growing aggregates may either be plastic, reorganizing for optimal molecular contact or kinetically trapped in a durable but poorly organized state. If the melting temperature of the side chains is below observation temperature, a 2D ordered liquid crystalline phase is observed [25]. Slow drying of films allows reorganization, while solvent remains as a plasticizer, and can yield a 3D ordered crystalline solid [21]. Films commonly dry too quickly for this process to finish, trapping an intermediate, partially crystalline structure within amorphous material

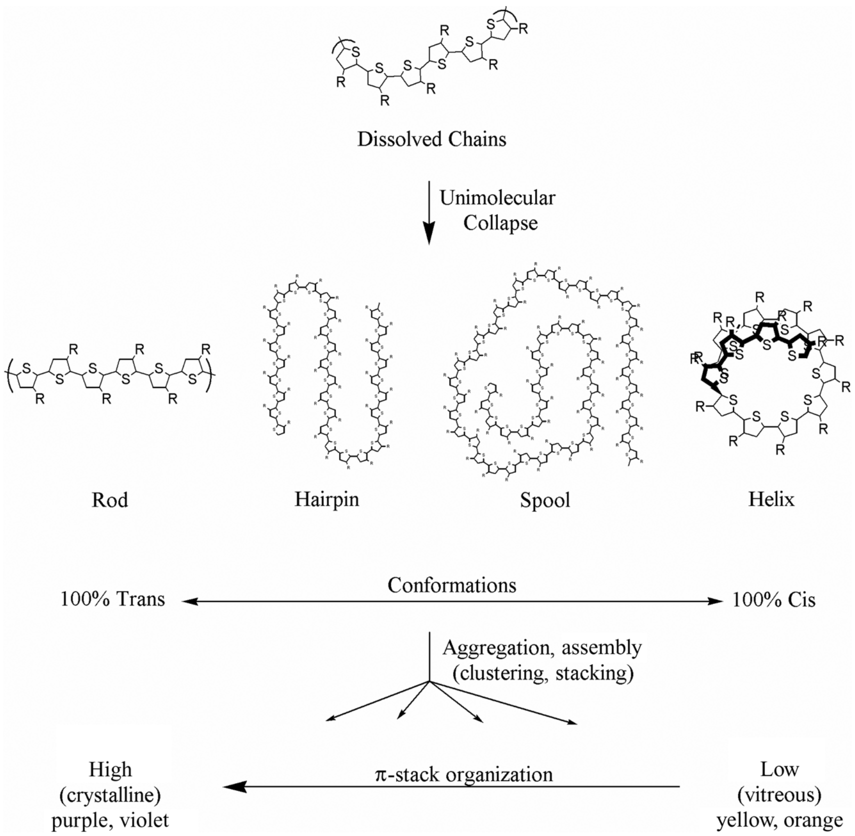

Figure 1.2 Possible molecular conformations and aggregation.

[26]. It is important to realize that in blends of rr-PT with other molecules in PV devices, that is, $C_{60}$ blends, the structural preferences for rr-PT do not go away and in most cases the rr-PT can dominate the structure and morphology, with the major change being only the domain size.

### 1.2.1
### Conformation

The molecular conformation of ir-PT and HT-PT in a good solvent is intermediate between ideal extremes of a random coil and rigid rod. The molecular conformation of rr-PT is also a mixture, with the rigid rodlike conformers dominating. The extent of enchained defects determines conformer bias in ir-PT. Sterically hindered HH couplings prevent coplanar orientation of rings, whereas HT and TT couplings allow both *cis*- and *trans*-coplanar orientation. A highly twisted ir-PT matches the volume and shape of polystyrene GPC standards more closely, giving comparable $M_w$ by light scattering and GPC [27], and exists as isolated chains in dilute THF [28]. A controversial point is whether eliminating defects gives rodlike conformers. Kiriy *et al.* note several structures allowing quasi-planar orientation of conjoined rings [29,30]. These can be imagined as a continuum from a linearly extended all-*trans*-planar (rod), through intermediates with increasing *cis* orientation, for example, folded ("hairpin") or coiled ("spool"), to an all-*cis* (helix) conformer. Recent STM studies on single molecules [31] and thin films of HT-PAT [32] verified both *trans*-planar (linear) and *cis*-planar (coiled) conformers are common in the solid state. Deviation of shape from a random coil causes GPC analysis, referenced to more spherical polystyrene standards, to consistently overestimate molecular weight by a factor of 1.8–2.0 [33].

### 1.2.2
### Aggregation

HT-regioregular polythiophenes aggregate even in good solvents. For example, HT-PDDT does not exist as dissolved, single chains even in dilute $CHCl_3$ solution near the boiling point. Aggregate shapes range from a disklike nematic liquid crystalline phase to needlelike structures with little two-dimensional order [25]. Stable colloidal suspensions in a solvent good for the alkyl chain but poor for the backbone (hexanes) have also been studied. This example of incomplete solvation caused unimolecular collapse followed by 1D aggregation into nanorods. Films made from solutions of rr-PTs in hexanes, spin cast on quartz, had an electronic spectrum comparable to the solution, indicating that the structure was conserved on deposition. Notably, the solution spectrum differed from the spectra of thin films spin cast from $CHCl_3$, confirming that different structures form under each protocol [30]. Rapid spin coating permits study of nonequilibrium structures by AFM at various stages of assembly [29,30]. Slow evaporation of extremely dilute solutions in a good solvent ($CHCl_3$) gave domains consistent with 1D assembly of linearly extended (all-*trans*) conformers. High concentration gave a lamellar network. In both, red-shifted optical absorption and vibronic structure indicate intermolecular interactions. The fluidity and amorphous nature of the alkyl side chains allows for reorientation from random coils in solution to linear rods in the solid state, and this mechanism adequately explains anisotropic assembly of crystalline domains. For example, very slow deposition from $CHCl_3$ allows the formation of well-defined "crystalline" nanorods with large (1 μm × 1 μm × 500 μm) dimensions [21].

In contrast, a nonsolvent (MeOH) drives unimolecular folding into poorly ordered flat structures at low concentrations [29,30]. Chain collapse was verified in a related PT derivative [34]. Concentration-independent vibronic structure indicating a molecular property is observed; higher concentrations give spherical agglomeration but no change in optical structure. Solvophobic interactions are minimized in a poor solvent by unimolecular collapse into planar, disklike objects that may further aggregate by cofacial stacking [29,30]. A good solvent for the alkyl chains seems to plasticize the molecules, allowing reorganization of the aggregate into domains with rodlike morphology. Colloidal solutions prepared by dissolving HT-PHT in $CHCl_3$ develop vibronic structure as solvent quality decreases [26]. Filtration removes this structure from the spectrum, leaving spectral features identical to polymer in good solvent and proving that aggregates are responsible.

### 1.2.3
### Solid Deposition

The deposition rate often determines to what extent molecules can organize. Spin casting deposits films with thicknesses correlating with initial solution concentration and spin speed [35], but varying rates of drying influence molecular assembly (Figure 1.3). Drop cast films can show little internal strain, whereas PHT spin cast

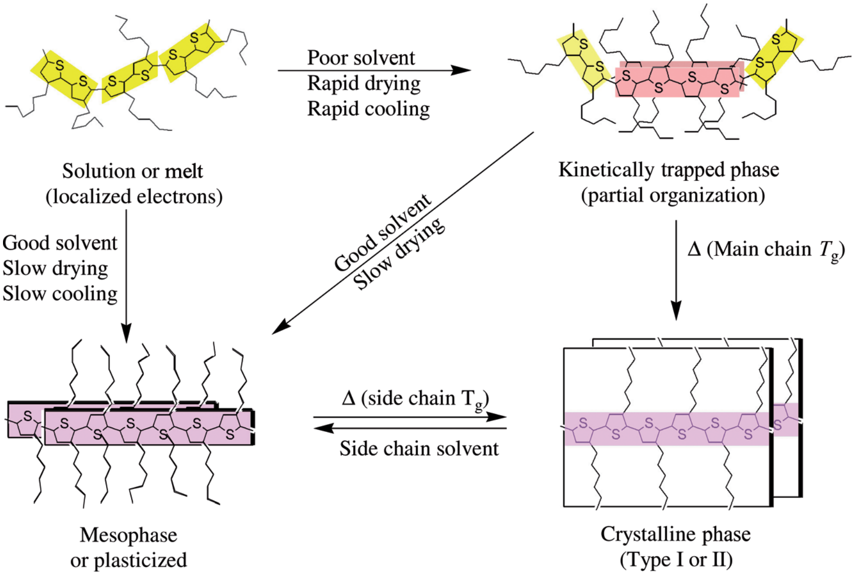

**Figure 1.3** Assembly of solid phases.

from xylenes or trichlorobenzene show strain increasing with spin speed and drying rate [17]. For the solvents studied, near maximal strain was reached at a spin rate of 3000 rpm. Importantly, no strain was seen in irregular samples. Energy can be released in a dramatic fashion: cutting the film with an AFM probe allows the edges to pull away, leaving trenches as wide as 2.3 μm. Slow drying promotes molecular assembly and relieves strain. Very slow deposition from a good solvent allows formation of well-defined "crystalline" nanorods [21] or, for narrow polydispersities, nanofibrils with domain width matching the length of the linearly extended molecule [12,24]. "Crystals" of PBT examined by SEM develop complex lamellar structure with layer thickness ranging from 15.6 to 104 nm, comparable to the 7 to 130 nm length distribution estimated from GPC measurements. Fractionation during a gradient crystallization process was proposed with each layer comprised of similar $M_w$ chains [24]. Clearly, the solution behavior at high concentration, for example, as solvent evaporates, is critical for obtaining well-defined solid-state domains.

### 1.2.4
### Solid-State Crystalline Order

When crystallinity in PAT is observed, chain association forms discrete lamellae of π-stacks (Figure 1.4). Microcrystalline domains are dispersed in a matrix of amorphous material. For 70% HT-PAT, with short HT–HT sequences [11], broad stacking distribution centers around 3.8 Å [36]. X-ray contour maps show weak diffraction in the small-angle region (1 0 0 peak). In the large-angle region, backbone scattering from segments with differing stacking distances generates a broad, amorphous halo (0 1 0 peak). In contrast, 98% HT-PT show a very narrow, well-defined ring at wide angles, indicating a well-organized narrow distribution around 3.81 Å [37]. The stacked structure is thought to be analogous in both materials. However, the entire HT-regioregular molecule can stack, eliminating poorly conductive, amorphous domains. Electrochemical doping of HT-PT can further compress stacks to 3.6 Å with compensating expansion along the 1 0 0 dimension to accommodate counter ions [38]. Packing disruption by HH linkage is seen in a 0% HT-PAT example (TT-HH). Large 4.4 Å *d*-spacing is too far to allow significant intermolecular π-orbital overlap, and lamellae of stacked molecules are not distinctly observed. Backbone association is very weak, suggesting that alkyl association drives order.

Two HT-PAT polymorphs have been characterized [39]. The most commonly observed and thermodynamically stable structure (Type I) develops with superposed π-systems 3.8 Å apart (Figure 1.4). A second polymorph (Type II), seen as a contaminant during solution casting or by crystallization near the side chain melting temperature [40], packs with 4.3 Å separation along the π-stacking axis and fully interdigitated alkyl chains. One morph seems to arise from the organizational preference of the backbone, and the other from the preference of the alkyl chain. Winokur's discussion of nanoscale structure–property relationships for conjugated polymers is a recommended overview [41].

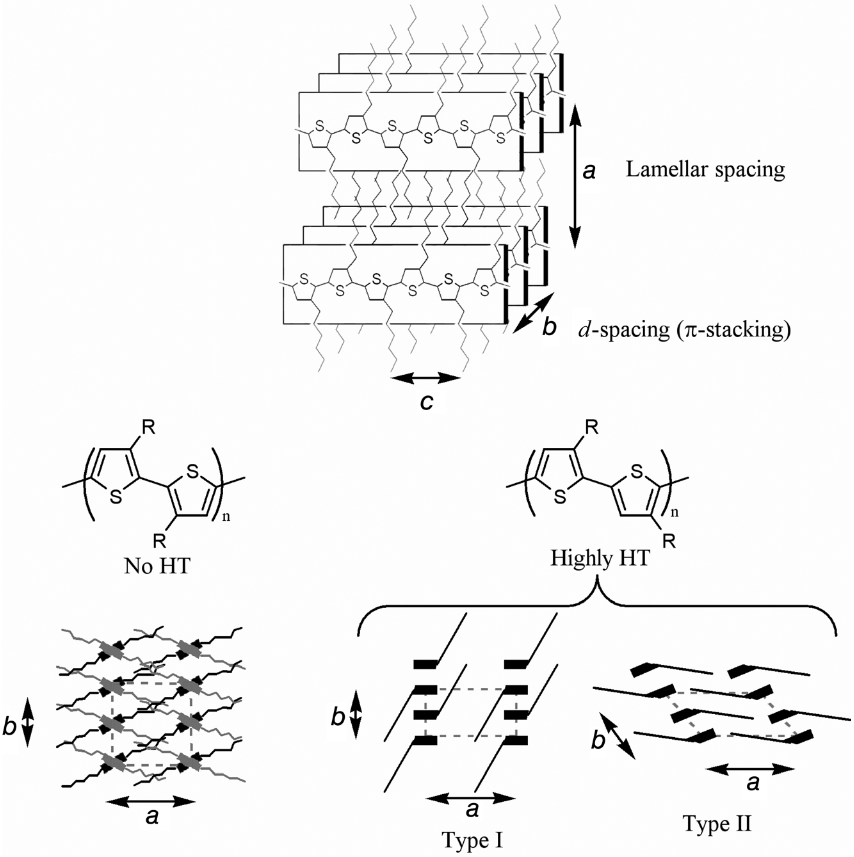

Figure 1.4 Crystal morphology in polythiophenes [39,232].

## 1.2.5
## Solid-State Phase Behavior and Thermal Analysis

Thermal behavior in rr-PTs is important, since thermal annealing of OPV films is common in the optimization. Processing conditions can kinetically trap material in one or more phases and varied domain sizes, giving variational thermal properties to the rr-PT films. Polythiophenes have added complexity from segregated aliphatic and aromatic components, and distinct transitions are possible for each. Representative data for several HT-PATs are summarized as a qualitative guide (Table 1.1). Glass transitions ($T_g$) are not commonly reported but seem to indicate both low- and high-temperature processes. Dividing data this way allows roughly linear correlation of changes in transition temperature versus alkyl chain length (Graph 1.1). For the sake of discussion, we refer to the low-temperature transitions as "side chain" melting and the high temperature as "backbone" melting for the reasons explained below. The most thoroughly characterized $T_g$ is for HT-PBT and correlates with the

**Table 1.1** Thermal characterization of poly(3-alkyl)thiophenes.

| | | | | Side chain | | Main chain | | |
|---|---|---|---|---|---|---|---|---|
| **Substituent** | **%HT** | **$M_n$** | **PDI** | **$T_{g1}$ (°C)** | **$T_{m1}$ (°C)** | **$T_{g2}$ (°C)** | **$T_{m2}$ (°C)** | **Reference** |
| $CH_3$ | ir-PT | — | — | — | — | 145 | — | [164] |
| $(CH_2)_3CH_3$ | ir-PT | — | | 75.4 | — | — | — | [45] |
| | >97 | — | — | — | — | — | 243 | [40] |
| | HT[a] | — | — | 67 | — | — | 272 | [42] |
| $(CH_2)_5CH_3$ | ir-PT | — | — | 12 | — | — | 178 | [165] |
| | 92 | $M_w = 8.7k$ | — | 20.3 | — | — | 222 | [166] |
| | | | | — | — | 110 | 230 | [167] |
| | >98.5 | $M_w = 50k$ | | — | 50 | 125 | 215 | [114] |
| $(CD_2)_5CD_3$ | HT[a] | 2582 | 1.40 | — | — | — | 46.3[b] | [168] |
| | | 7196 | 1.28 | — | — | — | 162.7[b] | [168] |
| | | 12 728 | 1.35 | — | — | — | 209.2[b] | [168] |
| | | 27 051 | 1.32 | — | — | — | 231.9[b] | [168] |
| $(CH_2)_7CH_3$ | ir-PT | — | — | 11.2 | — | — | — | [169] |
| | 89 | $M_w = 14.2k$ | — | −9.2 | — | — | 222 | [166] |
| | >98 | 11 900 | 1.34 | — | — | — | 175 | [170] |
| $(CH_2)_9CH_3$ | >99 | 3400 | 1.20 | — | 54, 68[c] | — | — | [171] |
| $(CH_2)_9CH_3$ | >99 | 14 100 | 1.64 | — | 44, 76 | — | 166 | [171] |
| $(CH_2)_{11}CH_3$ | ir-PT | — | — | 5.6 | 56.1 | — | 116.3 | [45] |
| | >98.5 | $M_w = 162k$ | — | — | 64 | — | 155 | [40] |
| | >98.5 | — | — | −19 | — | — | — | [172] |
| $(CH_2)_{15}CH_3$ | 98 | 14 000 | 1.61 | — | 93 | — | 145 | [170] |
| $(CH_2)_{21}CH_3$ | >95 | 7900 | 3.16 | — | 53.3, 70.6 | — | 103.8 | [173] |

[a] Not reported.
[b] Second heating.
[c] First heating.

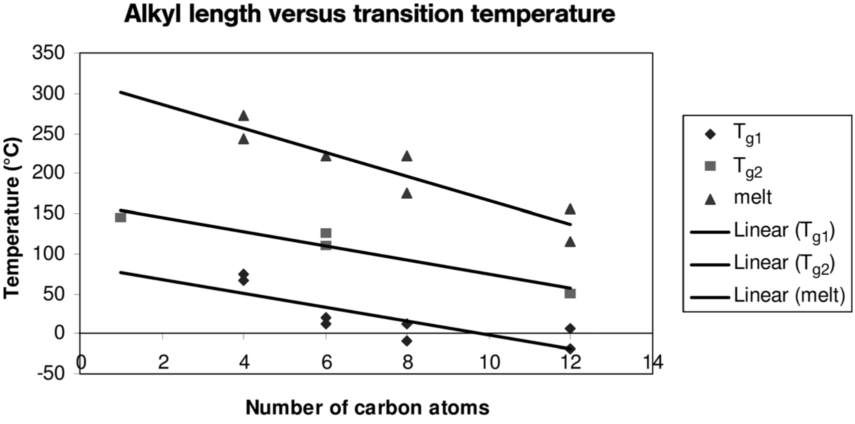

**Graph 1.1** Variation in transition temperature with alkyl chain length.

onset of backbone ring twisting [42]. Although occurring at high temperature, this "twist glass" transition seems best correlated with distal alkyl chain melting reported for other derivatives. In this series the slightly longer hexyl derivative has $T_g$ near room temperature (25 °C) and longer chains occurred below. A second, higher temperature glass transition has been reported in only a few cases. Though the data set is small, it seems correlated with $T_g$ reported for the methyl derivative. The latter cannot have two substituent-dependent processes and may be considered the structural archetype for thermal processes occurring only in the backbone. For PHT different studies reported either low or high $T_g$. No accounts describe both in the same sample; thus, it is unclear whether they arise from features of a common structure or from commingled phases. However, distinct glass transitions for (aliphatic) chain ends and the (aromatic) crystalline core of the mesophase are conceivable.

Melting ($T_m$) processes distinct for main chain and backbone have been reported. Side chain melting was not commonly observed for alkyl shorter than decyl; thus, they are excluded from the graph. When observed, it was at lower temperature than the backbone process and decreased with increasing alkyl length. The melting process may be imagined as melting of chain ends, with the π-stacked core remaining intact, giving a liquid crystalline mesophase [41]. Further heating expands the stacking distance in the core but does not eliminate crystallinity until melting [43]. A consequence of the two-phase model is that structural changes deriving from both regimes may be noted. In one example, graphs of OPV properties versus temperature show inflections near both transition temperatures [44].

Studies on ir-PT find that $FeCl_3$ doping raises $T_g$, possibly increasing organization in the quinoid form, but eliminates distinct melting [45]. Phase separation in blends was studied as a function of alkyl length and %HT [46–48]. Mixtures of HT-PAT with alkyl length differing by $C_4H_8$ clearly segregate. Smaller ($C_2H_4$) differences give seemingly stable blends until the proportion of the low-melting component becomes large, then phases separate. PHT ranging from 75 to 92% HT ($\Delta HT = 17$ mol%) cocrystallize, with melting temperature gradually increasing with HT content. Plasticizing additives are infrequently studied. Parity blends of HT-PHT or HT-POT with propylene carbonate melt at 80–120 °C lower temperature [49]. Polythiophene-based plasticizers designed with high HH content have been studied morphologically but not thermally characterized [50].

### 1.2.6
### Anisotropy

Mechanical and physical properties of polymers are determined largely by orientation. Efficient molecular alignment can maximize properties in one dimension by depleting it in others, to the extreme of being undetectable. For example, vibronic coupling, the intermolecular exciton, and intensity of the absorption spectrum are intense when measured parallel to the direction of polarization, along the long axis of the molecule. Measured orthogonal, the absorption is weak and unstructured, with the absorption maximum shifted to higher energy [20,51–55]. Extreme polarization affects all optoelectronic properties including conductivity [56], electron spin resonance (ESR) [57], vacuum UV [58], UV–Vis [20,26,51,59], spectroscopic ellipsometry [52–54], emission [29,54], IR, and Raman spectra [60]. Devices have been described with polarized electroluminescence [51], photoconductivity [55], photocarrier spin [61], and charge carrier mobility [62,63]. As domain organization improves, reducing isotropy, orientation control over large areas is needed to maximize properties including photon harvesting and charge transport. This permits optimization for specific device geometries. For example, conduction between laterally spaced source and drain electrodes in an FET requires π-stacking parallel to the (bottom) gate electrode, whereas solar cells need orthogonal alignment to connect vertically separated (top and bottom) electrodes. With respect to a surface, edge-on versus face-on orientation of π-orbitals in stacks tunes electronic contact at the interface from negligible to high, influencing charge transfer across the junction [64]. Ideally, orientation will be selected during processing and device assembly.

Bulk HT-polythiophenes can be modeled as crystalline domains imbedded in amorphous matrix. The nanocrystallites preferentially orient with one molecular surface in contact with the substrate, being isotropic in two rather than three dimensions in thin films. Slow deposition by drop casting orients molecules edge-on, with the π-stacking (*b*-axis) parallel to the substrate plane, in all samples studied including ir-PT. Depositing material faster, for example, by spin casting, skews molecular orientation from edge-on at low speeds to face-on at high speed [65]. Extremely fast spin casting precludes assembly, preventing significant reorganization of solvent-plasticized chains before solvent is lost, depositing poorly organized agglomerates. At temperatures below the side chain melt, a larger proportion of amorphous material is kinetically trapped. Observed polarization with deposition rate depends upon molecular substitution and regioregular structure, both critical parameters controlling assembly, and correlates with developing crystallinity [18]. Samples with >91% HT content and low molecular weight maintain the substrate parallel stacking motif. In contrast, samples with low regioregularity (81% HT) and high molecular weight orient the *b*-axis perpendicular to the surface. The effect clearly arises from HT content and $M_w$ rather than film thickness [1,66]. Epitaxial order persists only for a few monolayers, however. It is unclear whether solution aggregation alone or film organization at the meniscus of evaporating solvent is responsible [67]. Electrochemically deposited HT-PT films have the preferred orientation, with *b*-axis parallel to substrate, despite modifications of the unit cell including ~0.2 Å compression of the π-stack (*b*-axis) and ~1 Å expansion of the lamellar spacing (*a*-axis) [38,68,69].

Several methods have been studied to increase order in polythiophenes. Anisotropy can be increased locally, on the scale of one domain, through self-assembly on a surface to form nanowires. The crystallographic *b*-axis orients in the longitudinal dimension of the rod [21]. Solution crystallization forming filterable nanowires has also been proposed [70]. Alternatively, directional crystallization from a crystalline organic template orients π-stacks orthogonal to the long rod axis, with amorphous regions separating domains [22]. It is unclear whether the same assembly model applies in this case.

Macroscopic single domains have not been realized for rr-HTPT. Orientation of cast films over a large area by mechanical techniques can create significant polarity. In a simple example, physically robust, electrochemically prepared films may be physically stretched [59]. Highly regioregular polythiophenes are generally too brittle for this treatment and require painting onto a substrate that is then stretched [26]. Rubbing is another scalable, easily implemented technique. Microscopic areas ($10\,\mu m \times 10\,\mu m$) can be polarized by rubbing with an AFM tip [71]. On similar scale, stress created by drying and shrinkage of a superposed polymer creates a radial distribution of linearly polarized domains [19]. Larger areas of rr-PT rubbed with velvet become anisotropic, but ir-PT films do not [51,72]. A dichroic ratio of about 6 is observed in the photoluminescence. Shear and surface compression combine to orient 85% of crystalline domains along the rubbing direction, with the stacking axis orthogonal to the substrate [71]. Processing films in the plastic state, or while plasticized by evaporating solvent, provides additional control. Rubbing rr-PHT films with the edge of a quartz slide during casting from a high-boiling solvent (chlorobenzene, CB) aligns the $\pi$-stacking *b*-axis parallel to the substrate, and the crystallographic *c*-axis along the rubbing vector [55]. A method dubbed "friction transfer" draws a pellet of HT-PT across a substrate heated above the side chain melting temperature, depositing films >100 nm thick. Surface normal orientation of stacks with record dichroic ratio of 10–100 is accessible [20]. Application of ordering techniques in OPV blends has not been investigated to our knowledge.

## 1.3
## Characterization of Impurities

### 1.3.1
### Fractionation and Effects of $M_w$

Soxhlet extraction by increasingly "good" solvents provides a convenient means to separate impurities and narrowed $M_w$ fractions from broad polydisperse samples as has been shown by Pron. Solubility of HTPT increases in the following order: $CH_3OH < \text{acetone} < \text{hexane} < CH_2Cl_2 < \text{THF} < \text{xylene} < \text{chloroform}$ [73]. Successive fractions show increased $M_n$, $M_w$, and regioregularity, visible absorption $\lambda_{max}$ red shifting accordingly [73]. An ir-PHT prepared via $FeCl_3$ oxidation afforded fractions ranging from $M_n = 5k$ (75% HT; PDI = 1.6; $\lambda_{max} = 437$ nm) to $M_n = 34k$ (85% HT; PDI = 2.6; $\lambda_{max} = 443$ nm). Similarly, a commercial HT-PHT from Aldrich (Rieke) afforded fractions ranging from $M_n = 3k$ (81% HT; PDI = 1.3; $\lambda_{max} = 433$ nm) to $M_n = 33k$ (98% HT; PDI = 1.8; $\lambda_{max} = 452$ nm). Changing selectivity of the coupling reaction has been proposed to explain the trend toward higher HT content [26]. However, studies on metal-assisted cross couplings indicate no change in mechanism or selectivity is necessary to explain regioregular synthesis [13–15]. Chains initiated by a single TT defect subsequently grow by HT coupling. Defects are constant, at one per chain, becoming a steadily decreasing proportion of enchained couplings as $M_w$ increases.

A systematic study of bulk properties versus $M_w$ summarizes the changes [74]. Thin-film CV shows an oxidation at 0.74 V in all samples, decreasing with increasing $M_n$. Additional oxidations at 0.58–0.60 and 0.97–1.00 V, absent from ir-PHT and the acetone fraction (DP = 14), appear in the hexanes fraction (DP = 26) and intensify with $M_n$. Increased conjugation was proposed in agreement with red shifting of the solution UV–Vis $\lambda_{max}$ with increasing $M_n$. Solid-state spectra trend similarly but develop vibronic structure. The ~2.09 eV interchain exciton proposed by Brown and coworkers [75] appears in thin films of the hexanes fraction, intensifying with increasing DP. This parallels improving nanofibril width and order reported for increasing $M_n$ [12].

### 1.3.2
### Inorganic Impurities

Commercial availability of clean, well-characterized HT-PAT obviates the need for synthesis. However, all commercial rr-PTs are not the same and care must be taken to know the PDIs, the level of impurities, and the degree of regioregularity. Samples from Plextronics or Plexcore from Aldrich are examples of a very high grade of rr-PT. Molecular characterization has been reviewed [2–4]. Subsequent analysis by MALDI-MS, yielding correction factors (1.8–2.0) for molecular weight determinations by GPC, should be noted [33]. The characterization of inorganic impurities is less well addressed, leaving their effect uncertain. Some report devices made with commercial HT-PT, as received, can be as good or better than purified samples, though the device lifetime is not mentioned [76]. Others find that impurities can limit charge carrier mobility [77,78] or give additional peaks in the DSC thermogram [76]. Adsorption into nanoporous $TiO_2$ is electrostatically hindered, requiring fractionation for maximal HT-PT infiltration [79]. The crude product of polymerization contains phosphine ligands, from the catalyst, and inorganic salts. By-product zinc bromide (from some synthetic methods) salts modify the absorption spectrum and partially quench fluorescence. Some commercially obtained samples with this problem contained high residual Zn ($6.1 \times 10^{-6}$%) and Br ($6.4 \times 10^{-6}$%) levels [80]. Soxhlet extraction with methanol (24 h) then hexanes (24 h) reduced Zn to negligible concentration, and only bromine associated with chain ends remained. Others note similar problems with ash as in the elemental analysis could not be simply resolved by precipitating from a good solvent ($CHCl_3$) into a poor solvent (MeOH) unless dilute solutions and long times were used [81]. Chelation seems an effective general method for removing Pd, Cu, Ni, and metallic residues [82,83].

Molecular oxygen commonly contaminates by forming charge transfer complexes with polythiophene [84]. Exposing a 100 nm HT-PHT film to air for a few seconds raises conductivity four orders of magnitude to its equilibrium value [85]. Oxygen-doping effects include a broad, low energy absorption in the visible spectrum ($\lambda_{max} \sim 1.97$ eV; 629 nm) and radicals detected by EPR [84]. In diodes exposed to oxygen in the dark mild doping causes a shift of the flat band voltage [86]. Light exposure increases doping efficiency with greatest effect near the absorption maximum of the charge transfer complex. However, charge carrier density is unstable, continually increasing during the ~1 h experiment. Photobleaching is possible in organic solvents (not in OPVs due to fast electron transfer to $C_{60}$) under certain conditions, but chain cleavage requires metal contaminants [87]. Several methods have been proposed to remove oxygen from films. Annealing above 100 °C in inert atmosphere reduced oxygen content below limits detectable by Rutherford backscattering spectrometry (RBS) [88,89]. Heating HT-PHT in vacuum (147 °C) reduced conductivity by four orders of magnitude but several hours were necessary to render conductivity negligible [85]. Chemical dedoping with tetrakisdimethylaminoethylene neutralized charge carriers, reducing conductivity from $\sigma = 3 \times 10^{-5}$ to $\sigma = 5 \times 10^{-10}\,\mathrm{S\,cm^{-1}}$ [90]. Deoxygenation of prepared FET structures by applying a negative gate bias was also reported [91].

## 1.4
## Optical and Electronic Properties of PAT

### 1.4.1
### Optical Properties: Intermolecular Excitons

Optical absorption of HT-PT depends upon substituent inductive effects, chain twisting, and chain association. This was reviewed [2–4] before the discovery of the intermolecular exciton band [75]. Samples with varying %HT show intensified absorption at 2.09 eV as defects decrease. This feature was present in all ir-PT and HT-PT, at constant energy, and was not completely bleached by heating or changing solvent quality. A neutral (Frenkel type) interchain exciton was proposed. Intensity of this absorption is correlated with the microstructural order in the polymer and diminished as HH defect content increased. The improved interchain interaction in HT-regioregular P3AT demonstrates transformation from classical unimolecular, one-dimensional properties to quasi-two-dimensional behavior.

The conjugation length independent exciton absorption implies that HOMO–LUMO gap estimation from UV–Vis absorption band edge can be misleading, identifying a low energy process accessible to only a fraction of the bulk material. This interchain process is the lowest energy absorption present in ir-PT but is much more intense in self-assembled HT-PT; the bandwidth is larger, implying higher mobility. This parameter seems useful for comparing disparate samples with different (or unknown) thermal histories. In a recent study of properties versus chain length, fractionated HT-PHT was spin coated from $CHCl_3$ onto glass [92]. Retroanalysis of thin-film absorption spectra indicates varying intensities of the 2.07 eV (593 nm) interchain exciton, seeming to be correlated with the degree of crystallinity, in all but the lowest $M_w$ fraction. However, X-ray studies of the films showed a well-resolved 1 0 0 lamellar spacing only in the high $M_w$ fraction. Annealing at high temperature developed the 1 0 0 peak in all fractions [92]. The initial difference may reflect solid-state structure derived from preorganized aggregates, detected by the 2.09 eV absorption. Either the processing or the structure of the high $M_w$ fraction promotes formation of nanocrystalline domains in solution that may template further organization on drying.

### 1.4.2
### HT-PT Electron Transport: Conductivity and Mobility

Conductivity in organic semiconductors depends on generating efficient pathways through the bulk. Irregular PATs have the disadvantage in this regard, with conductivities typically on the order of $\sigma = 0.1\text{–}1.0\ \mathrm{S\,cm^{-1}}$ when doped with iodine. In contrast, HT-PAT conductivities typically are $\sigma = 100\text{–}200\ \mathrm{S\,cm^{-1}}$ with some samples as high as $1000\ \mathrm{S\,cm^{-1}}$ [2–4]. Balanced TOF carrier mobility for carefully cleaned HT-PHT, spin cast from $CHCl_3$ onto ITO, shows hole mobility $\mu_h = 3 \times 10^{-4}\ \mathrm{cm^2\,V^{-1}\,s^{-1}}$ and electron mobility $\mu_e = 1.5 \times 10^{-4}\ \mathrm{cm^2\,V^{-1}\,s^{-1}}$ [77]. Controlling donor and acceptor mobility is important for optimization of the OPV device, since the charge separation and generated current will depend on a balance.

## 1.5
## Benefits of HT-Regioregular Polythiophenes in Solar Cells

Contemporary photocurrent generation and device design are addressed in detail elsewhere in this book. The following discussion of photocurrent generation considers four processes: (i) light absorption, generating an exciton; (ii) exciton diffusion (to an interface); (iii) charge separation into independent holes and electrons; and (iv) charge conduction to an electrode (Figure 1.5). Competing processes, depicted in blue, include exciton recombination and electron back transfer from the acceptor to the donor. In this model, there are several advantages of HT-regioregular polythiophenes over other p-type organic semiconductors. Polythiophenes are strong

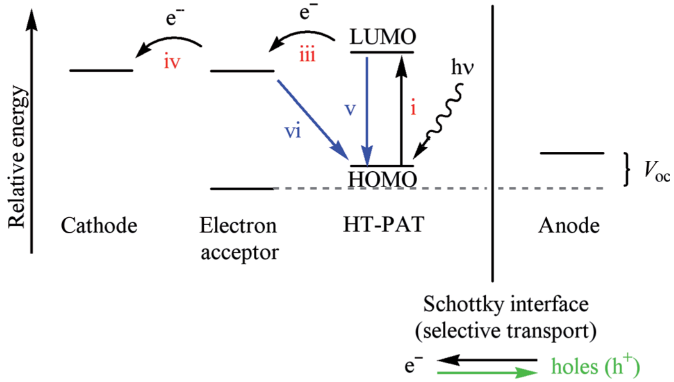

**Figure 1.5** Simplified photocurrent generation mechanism: (i) absorption, (ii) exciton diffusion (not shown), (iii) charge separation, and (iv) conduction; competing processes include (v) recombination/relaxation and (vi) electron back transfer.

absorbers with a broad absorbance profile. Domains with extended π-stacking support intermolecular excitons, responsible for much of the low energy absorption, with absorption most intense in self-assembled HT-PT [75]. The spectral window is effectively widened. Blending with n-type semiconductors expands this further by introducing additional molecular and charge-transfer absorptions. For example, blending 1 : 1 with phenyl-$C_{61}$-butyric acid methyl ester (PCBM) increases absorption into the UV and infrared [93]. Spontaneous polymer assembly, occurring even under mild heating, generates domains with high charge carrier mobility – aiding charge separation and conduction to an electrode. Consequent anisotropy suggests polarization effects (e.g., directionally optimized transport) become important in phase-separated heterojunctions.

## 1.6
## Bulk Heterojunctions: Focus on HT-PAT/PCBM Blends

The discovery of fast, efficient photoinduced electron transfer from electron-rich conjugated polymers to fullerenes inspired the creation of polymer-based solar cells [94]. Studies were initially hampered by low solubility and a tendency for crystallization, but solubilizing substituents largely reduced these difficulties, albeit while adding the prospect of polymorphism effecting device performance [95]. Successful implementation in photovoltaic devices requires processing conditions controlling phase and domain (crystallite) size. In the context of the above structural propensities of rr-PT, the assembly of HT-PT into nanocrystalline domains with its partner fullerene is critical for efficient OPVs. Hierarchical assembly by fullerene derivatives and resultant structural motifs invites more extensive discussion than given here and more importantly more structural work on rr-PT/fullerene blends. Recent developments of liquid fullerene derivatives, one-, two-, and three-dimensional ordered solids, are recommended starting points for further study [227–229]. This section focuses on PCBM and blends with HT-PAT as a currently popular research target to understand processing parameters optimizing OPV performance. Properties of photovoltaic devices incorporating HT-regioregular polythiophenes and reported in the past 5 years are surveyed in Appendix 1.A.

### 1.6.1
### Homogeneous PCBM Assembly

It is useful to understand the innate behavior of PCBM, before studying its behavior in blends, as the archetype of the segregated phase in heterojunction devices. As received, PCBM powder diffracts well [96] but thin films spin cast from $CHCl_3$ are amorphous, even after annealing (12 h, 100 °C) [96,97]. Crystalline organization has been studied by Yang *et al.* [98]. Thin films spin cast from toluene (Tol) or chlorobenzene, formed by homogeneously distributed small molecular aggregates, were mechanically stable and separable from the substrate. Substantial variations in thickness were evident in the Tol cast film, suggesting that CB is a poorer solvent from

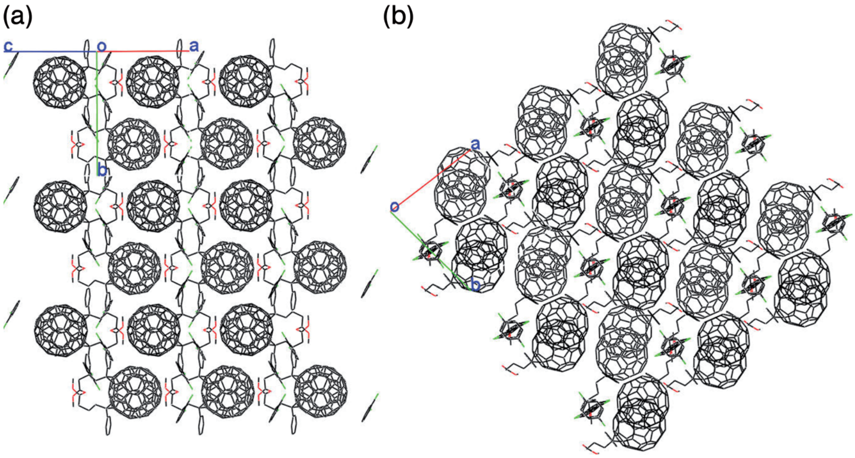

**Figure 1.6** PCBM crystal packing, 3 × 3 × 3 unit cells.
(a) Dichlorobenzene solvate viewed along [1 0 −1] plane;
(b) chlorobenzene solvate viewed along [1 1 0] plane.

which crystals form. Reducing the rate of solvent evaporation by drop-casting films prevented discrete film formation. Large aggregates with darker (more dense) clusters developed instead. Slow solvent evaporation under saturated atmosphere allowed crystal growth to several micrometers in size. Small crystals, on the order of 0.5 μm long, were grown by annealing spin-cast samples (50 h/130 °C). Selected area electron diffraction (SAED) analysis of each product showed concentric rings from tiny crystallites in spin-cast films that evolved to a distinct pattern of well-aligned spots as the crystallite size increased. Three major Debye–Scherrer diffraction rings, with *d*-spacing of 4.6, 3.1, and 2.1 Å, resolved into several reflections with similar *d*-spacing. The authors found no concurrence with published crystal structures, but concluded that the same crystal phase was present in all samples, even upon annealing, with crystallite size changing as a function of processing conditions. Rispens *et al*. reported that distinct crystal structures can arise from different solvents [95]. Structurally, both sample phases separate into wavy, fullerene-rich domains and its methano-ester/solvent-rich domains (Figure 1.6). Samples crystallized from DCB are clearly lamellar, implying poor electronic connection between fullerene layers. In contrast, samples crystallized from CB periodically touch and improve connectivity. Solar cells with active layers spin cast from CB showed higher $I_{sc}$ and efficiency than those cast from DCB or xylenes, implying that PCBM organization was responsible.

### 1.6.2
### HT-PAT/PCBM Blends: Component Ratio

Optical absorption spectra of spin-cast 50 wt% HT-PDDT/fullerene mixtures are a simple composite of the component spectra, indicating negligible ground-state charge transfer [99]. Blending hinders self-assembly during deposition, reducing absorption attributable to the nanocrystalline phase. Absorption intensities of PCBM/HT-PHT blended films, spin cast from DCB, decrease and absorption maxima blue shift, relative to pristine polymer, because of PT disordering. For >67% PCBM blends, nonphotoinduced charge transfer complexes become important [100]. Charge carrier generation efficiency in blends changes little in comparison to pristine polymer. Rather, the primary effect in >50% PCBM is the increased charge carrier lifetime. In PHT-rich phases (80–100%) the majority of charge carriers are short lived (10–15 ps); in 50% and lower blends new, long-lived (>500 ps) carriers appear, attributable to interfacial charge separated species [101]. The longer lifetime increases, the distance carriers can diffuse before quenching, increasing the probability of separated charge reaching an electrode. Charge transport is dispersive (non-Gaussian) for extreme compositions where short lifetimes dominate. Nondispersive (Gaussian) transport is observed in the narrow composition range (44% < PHT 77%), giving the highest photocurrent lifetimes. Qualitatively, nondispersive photocurrent profiles correlate with better structural order, while dispersive transport is observed for extreme phase segregation [102].

Current density is generally highest in 1 : 1 blends [100,103–105]. Decreasing PCBM content from 75 to 41 wt% is reported to improve diode characteristics, though $V_{oc}$ remains stable [106]. There are conflicting reports of fill factor (FF) evolution versus component ratio under identical thermal processing. One study finds a maximum at 47–50% PCBM with poor performance of higher ratios attributed to fullerene crystallization [106]. Another study of thickness-optimized films reports gradual increase in efficiency as PCBM content increases from 30 to 60% [105].

## 1.6.3
## HT-PAT/PCBM Blends: Annealing

### 1.6.3.1 PCBM Phase Separation and Assembly

High mobilities reported for electrons in PCBM ($\mu_e = 2 \times 10^{-3}\,\mathrm{cm^2\,V^{-1}\,s^{-1}}$ [107]) and holes in assembled HT-PHT fibrils ($\mu_h = 1 \times 10^{-2}\,\mathrm{cm^2\,V^{-1}\,s^{-1}}$ [12]) indicate suitably complimentary charge carrier materials, provided phase assembly yields effective pathways. Annealing blends below the polymer $T_{g2}$ limits diffusion and assembly of the fullerene phase. Devices with 1 : 2 PHT:PCBM films heated to 90 °C seem to reach a stable morphology after ~20 min, with little change in efficiency during 15 min additional anneal. Heating above $T_{g2}$ (150 °C) causes a sharp efficiency spike followed by collapse to nearly zero [108]. For 1 : 1 PHT:PCBM films above $T_{g2}$ (130 °C, 30 min) 9 μm PCBM crystals form [109]. This temperature-dependent behavior, seen in different compositions, reflects sharply increased fullerene mobility through the flexible polymer composite. Crystal growth in $CHCl_3$ cast films has been thoroughly studied, indicating that temperature, rather than time, determines the ultimate size of PCBM crystallites [110]. Brief annealing (20 s/130 °C) of 50–60% PCBM yielded tiny, isolated crystallites, but for 67–75% large grains formed [106]. Slightly longer annealing of 1 : 1 films (130 °C/5 min) generated >10 μm PCBM crystals and 10–30 nm dark spots, thought to be PCBM-rich clusters, homogeneously distributed